Chinese Chemical Letters 35 (2024) 108707

Contents lists available at ScienceDirect

Chinese Chemical Letters

journal homepage: www.elsevier.com/locate/cclet

Lead-free hybrid two-dimensional double perovskite with switchable dielectric phase transition

Tian Yang[a,b], Yi Liu[b,*], Lina Hua[a,b], Yaoyao Chen[a,b], Wuqian Guo[b], Haojie Xu[b], Xi Zeng[b], Changhao Gao[a,b], Wenjing Li[b], Junhua Luo[a,b], Zhihua Sun[a,b,*]

[a] College of Chemistry, Fuzhou University, Fuzhou 350108, China
[b] State Key Laboratory of Structural Chemistry, Fujian Institute of Research on the Structure of Matter, Chinese Academy of Sciences, Fuzhou 350002, China

ARTICLE INFO

Article history:
Received 17 April 2023
Revised 19 May 2023
Accepted 19 June 2023
Available online 25 June 2023

Keywords:
Dielectric switch
Lead-free
Double perovskite
Phase transition
Symmetry breaking

ABSTRACT

Molecular dielectric switches constitute a type of intelligent materials that are highly coveted for their distinctive advantages of switchable dielectric responses, lightweight, and mechanical flexibility. Two-dimensional (2D) hybrid perovskites have demonstrated excellent promise for assembling dielectric switches, in which the dynamic motions of organic moieties afford driving force to trigger switchable dielectric phase transition. Here, we successfully assembled a new lead-free hybrid double perovskite, $(CHA)_4CuBiBr_8$ (**1**, CHA = cyclohexylammonium), adopting a typical 2D structural motif, which shows dielectric anisotropy and bistable behaviors during the reversible phase transition near $T_c = 378$ K (the Curie temperature). That is, its dielectric constants could be switched and tuned between high-dielectric and low-dielectric states. Structure analyses reveal that the ordered-disordered transformation of the organic CHA^+ moiety and distortion of inorganic framework account for its phase transition. This result will stimulate further exploration of molecular dielectric switches in this 2D environmentally friendly family.

Dielectric switches, which enable the reversible switching of the dielectric constants between high and low dielectric states, are garnering significant interest because of their potential application, such as data storage, signal processing and actuator [1–6]. From a microscopic perspective, this variable dielectric permittivity results from the reconfiguration of structural elements between the static and dynamic phases, which is possibly achieved through a structural phase transition [7]. Recently, substantial studies have been carried out on structural phase transitions to explore molecular-based materials with remarkable switchable dielectric properties, including pure organic crystals [8], crown ether clathrates [9], and organic binary salts, *etc*. [10–13]. These molecule-based phase transition materials with inherent superiorities in structural tunability and facile processability are booming as the potential alternatives of dielectric switches. For instance, the organic-inorganic hybrid complexes $[C_5H_{10}NH_2]_2BiX_5$ (X = Cl and Br) exhibit the switchable dielectric behaviors from the low-temperature low dielectric constant (ε') state to high-temperature high dielectric constant (ε') state, attributing to the structural phase transition triggered by the dynamic motion of the cations [14–16]. Interestingly, the dielectric switching properties of these hybrid compounds can be significantly improved by the component regulation, such as phase transition temperature and switching ratio of dielectric constants. Therefore, it is promising to exploit high-performance switchable functional materials by virtue of reasonably assembling new dielectric switches associated with phase transition.

Two-dimensional (2D) organic-inorganic hybrid perovskites demonstrate distinctive chemical variability and accompanying structural adaptability, rendering them highly attractive candidates for novel switchable dielectric-active materials [17–23]. In particular, the onset of dielectric phase transition is intimately linked with the order-disorder structure changes of organic cations, which confer switchable dielectric responses between two distinct dielectric states. Although 2D single-metal hybrid perovskites have achieved great progress in the field of dielectric switches [24–31], most of them contain toxic element of Pb^{2+} cation, which hinders their further practical applications. By contrast, the mainstream of the metal-halide double perovskites with nontoxic heterovalent metal cations is occupied by 3D systems, such as $Cs_2AgBiBr_6$ [32–34], $Cs_2AgSbBr_6$ [35] and $(MA)_2AgBiBr_6$ [36], which are only compatible with small-size cations, restricting the generation of structural phase transition and affecting the acquisition of dielectric switch materials. Consequently, it is extremely challenging and meaningful to explore new 2D hybrid double perovskites, which combine

* Corresponding authors.
E-mail addresses: liuyi@fjirsm.ac.cn (Y. Liu), sunzhihua@fjirsm.ac.cn (Z. Sun).

https://doi.org/10.1016/j.cclet.2023.108707
1001-8417/

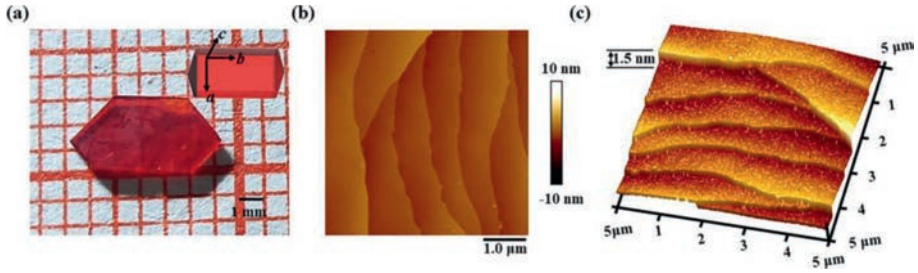

Fig. 1. (a) The crystal photographs for compound **1**, inset is the crystal morphology. AFM (b) 2D and (c) 3D images of the surface of single crystal.

the structural variability of flexible organic cations with the composition tunability of inorganic skeleton, possessing an inspiring future for the creation of stable and environmentally favorable molecular dielectric switches.

Here, we designed a new 2D lead-free hybrid double perovskite $(CHA)_4CuBiBr_8$ (**1**, CHA = cyclohexylammonium). Structurally, the order-disorder transformation of the organic CHA^+ moiety cooperating with the distortion of the inorganic framework give rise to its striking dielectric bistable and anisotropic behaviors around the phase transition temperature of 378 K. Particularly, **1** exhibit a stable transition between the high and low states over multiple cycles, indicating its excellent durability of dielectric response. Such unique characteristics arouse the potentials of **1** in dielectric switch fields and would promote the development of "green" switching devices.

All chemical reagents used were of analytical reagent grade, for which the purity was greater than 99%. Firstly, compound $(CHA)_4CuBiBr_8$ was synthesized from hydrobromic acid solution containing cyclohexylamine, Cu_2O and Bi_2O_3 with the stoichiometric ratio of 8:1:1. In order to obtain large-size single crystals, we controlled the solution temperature with the cooling rate of 1 K per day, and large red crystals were easily obtained after two months (Fig. 1a). The powder X-ray diffraction (PXRD) pattern of **1** at ambient temperature (Figs. S1 and S2 in Supporting information), was found to closely match with the calculated data based on the crystal structure at 298 K, confirming the phase purity and stability of as-grown crystals.

The supporting information provides a thorough explanation of the techniques for single-crystal X-ray diffraction, PXRD, dielectric, differential scanning calorimetry (DSC), thermogravimetric analysis (TGA), and optical measurements.

Block red crystal of **1** was obtained by cooling the precursor solution from 353 K to 300 K. Moreover, its crystal morphology coincides with the predicted result from its single-crystal structure (Fig. 1a). Additionally, the AFM experiment was used to examine the surface microstructure of **1**. The smooth surface of the crystal has no apparent holes, as shown in the 2D image, clearly revealing its monocrystalline characteristics (Fig. 1b). It is not difficult to see that cationic and inorganic layers are arranged alternately to form a 2D monolayer structure along the *a*-axis. Interestingly, the 3D image of crystal surface shows that there is a step-like growth morphology, which just fits in with the layered growth of 2D organic-inorganic hybrid perovskite, and the crystal grows along the step (Fig. 1c).

During differential scanning calorimetry (DSC) measurement, the endothermic and exothermic peaks of the heating and cooling cycles are indicative of a reversible phase transition. As shown in Fig. 2a, the temperature profiles during heating and cooling show a pair of reversible peaks, that is, the endothermic and exothermic peaks observed at 388 and 378 K, respectively. Such DSC results solidly demonstrate the reversible phase change of **1**. Interestingly, the phase transition temperature is higher than room temperature, but far from its decomposition point ~563 K (as shown in the TGA curve, Fig. S3 in Supporting information). This high phase transition temperature might benefit its potential applications in the high-temperature condition. Subsequently, we designate the temperature range prior to the phase transformation as the low temperature phase (LTP), and the temperature range subsequent to the phase transformation as the high temperature phase (HTP).

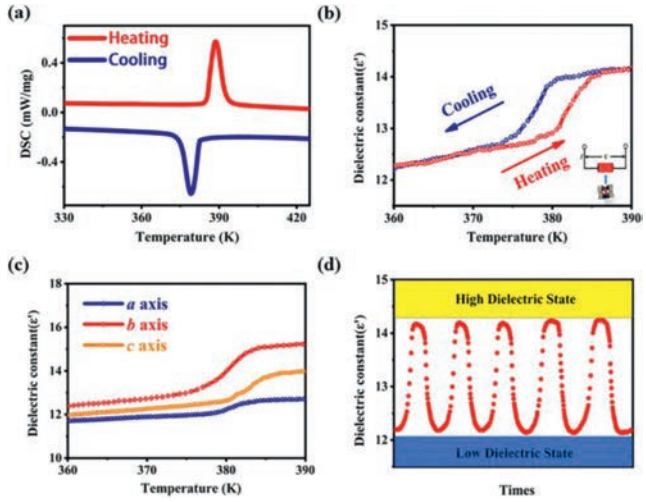

Fig. 2. (a) DSC curves of **1** in heating-cooling runs. (b) Temperature-driven ε' switching of the crystal during heating and cooling at a frequency of 1 MHz. (c) Dielectric properties along different axes at 1 MHz upon cooling. (d) Cycles of transitioning between the high and low dielectric states of ε' at a frequency of 1 MHz.

Phase transitions with the dielectric variations provide a potential platform for exploring switchable dielectrics. A crucial characteristic of phase transition materials is the variable dielectric constant (ε'). Fig. S4 (Supporting information) depicts the temperature-dependent permittivity of powder for compound **1** at different frequencies. Below 380 K, the ε' value keeps a slow increase at the frequencies of 300 kHz, 500 kHz and 1 MHz. Upon heating to 390 K, a remarkable step-like anomaly manifests the phase transition. The ε' result encounters a plateau with a modest enhancement with the temperature raising further. Fig. 2b shows the temperature-driven switching of ε' values under the frequency of 1 MHz by heating and cooling of the crystal. These two separate dielectric states for **1**, the low-dielectric phase (below T_c) and the high-dielectric phase (above T_c), suggest the characteristic of dielectric switches.

Furthermore, the single-crystal sample was used to study the exceptional anisotropy along the various crystallographic axes. The temperature-dependent permittivity obtained by applying voltage along different axes of crystal **1** at the frequency of 1 MHz (Fig. 2c). Emphatically, along *b*- and *c*-axis directions, the permittivity is larger than that of *a*-axis direction, which suggests an intrinsic anisotropy for **1** along different axes. Compound **1** has the potential to be a switchable dielectric material due to its dielectric

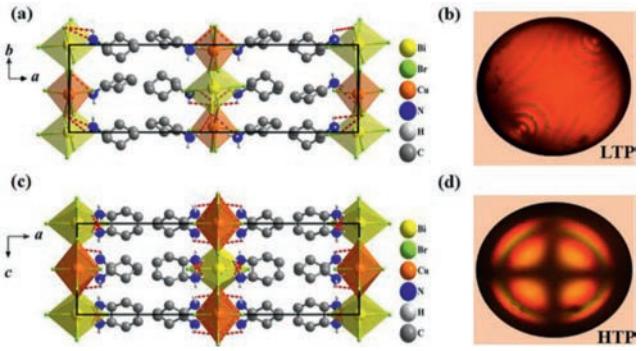

Fig. 3. The crystal structure of **1** at (a) 300 K and (c) 378 K. Optical axis in (b) LTP and (d) HTP.

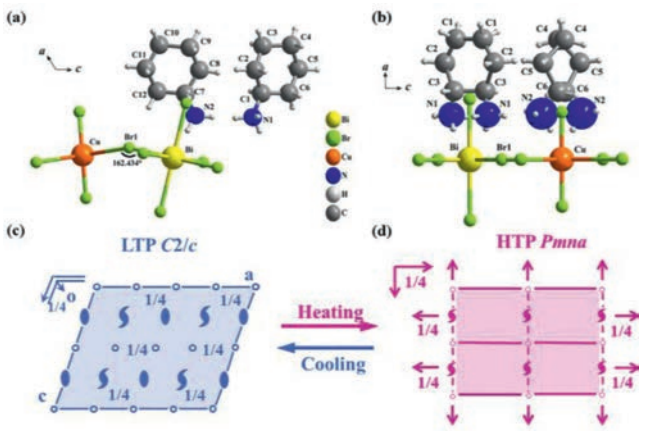

Fig. 4. The asymmetric unit of **1** in the (a) LTP and (b) HTP, and (c, d) symmetry transformation of **1** during the phase transition.

switching characteristics between the states of high and low dielectric. A crucial measurement for assessing performance is the switching repeatability. For **1**, numerous cycles with the reversible switching of dielectric constants were also carried out to demonstrate the stability of the conversion from the high dielectric state to low dielectric state. A small rise of around 14 is maintained in the HTP, which is consistent with the high dielectric state. There is almost no time delay as the temperature drops, while the ε' quickly drops from 14 to 12, signifying the low dielectric state. The dielectric signals in Fig. 2d exhibit a stable transition between the high and low states over multiple cycles, even with the passage of time and consistent temperature changes. These important findings demonstrate that **1** possesses certain advantages in terms of stability, indicating its potential for application in temperature-sensitive systems.

At 300 K (LTP, CCDC: 2256278) and 388 K (HTP, CCDC: 2256895), single-crystal X-ray diffraction experiments were performed to explore the mechanism of the phase transition of **1**. From the packing structure (Figs. 3a and c), the metal-halide $BiBr_6$ and $CuBr_6$ octahedra spread along the *bc* plane, thus constructing a 2D inorganic perovskite framework. There are double layers of cyclohexylamine cations between the monolayer inorganic framework, which adopts a typical Ruddlesden-Popper layered structure. Compared with the single-metal perovskites, double perovskite structures show different structural adjustability. The coordination of its perovskite framework can be regulated by assembling different kinds of heterovalent metal cations to improve physical properties, such as phase transition temperature, optical absorption and band gap [37–39]. From the structure viewpoint, the N–H groups of organic CHA^+ cations form N–H···Br hydrogen bonds with the Br^- ions of inorganic $CuBr_6$ and $BiBr_6$ octahedra. The close proximity of CHA^+ cations to $CuBr_6$ and $BiBr_6$ octahedra facilitates the formation of such hydrogen bonds with the lengths ranging from 3.3 Å to 3.5 Å (Fig. 3 and Table S6 in Supporting information). These hydrogen bonding interactions play an important role to stabilize the crystal structure of **1** [40,41]. During phase transition, the obvious changes in its crystallographic data can also be used to understand these striking distinctions between LTP and HTP structures. Specifically, in the LTP, **1** crystallizes in the monoclinic space group *C*2/*c* (Fig. 3a), but undergoes a phase transformation into the orthorhombic system with the space group *Pmna* (Fig. 3c). Under a polarizing microscope, the optical axis clearly demonstrates the evolution from biaxial nematic phase (Fig. 3b, LTP) to the uniaxial phase (Fig. 3d, HTP), being consistent with a structural phase transition from 2/*m* to *mmm*. Meanwhile, with the crystal changing from an optically biaxial condition to a uniaxial state, the color variation of **1** has been directly observed during this process (Fig. S5 in Supporting information).

Subsequently, the dynamic transformation of organic cation and inorganic skeleton during phase transition is analyzed in detail. In the LTP, all of the cyclohexylamine atoms are in an ordered form (Fig. 4a). All the atoms are distributed in the exclusive occupations, and the C–C bond lengths and bond angles are homogeneous. It is clear that the metal-halide $CuBr_6$ octahedra have an obvious distortion, as deduced from the Cu-Br bond lengths and Br-Cu-Br bond angles at LTP. For instance, the Cu-Br-Bi bond angle is 162.434°, revealing the small-angle tilting motion. As depicted in Fig. 4b in the HTP, the C and N atoms appear helically symmetrical in two planes from two directions, and the C atoms become strikingly disordered and occupy two equivalent disordered positions. Moreover, thermal ellipsoids of N atoms at HTP are much larger than that at LTP, and the Br-Cu-Br and Br-Bi-Br bond angles change to be equivalent. These variations indicate that the symmetry of the $CuBr_6$ and $BiBr_6$ octahedra anion were elevated with the temperature increasing from the LTP to HTP. The crystallographic symmetry of **1** breaks from the highly-symmetric point group *mmm* to the low symmetry of 2/*m*, namely, symmetry breaking. As a result, the number of symmetric components is reduced by half from eight (i, C_2, $2C_2$, E, σ_h, $2\sigma_v$) to four (E, i, C_2, σ_h), which corresponds to the Landau phase transition theory (Figs. 4c and d) [42–44].

Based on the layered structure of 2D hybrid double perovskite, we measured the ultraviolet-visible (UV–vis) diffuse reflectance of **1** (Fig. 5a). The optical absorption spectrum shows a sharp cutoff at 480 nm, from which its optical bandgap was deduced as 2.58 eV by fitting the *Tauc* equation. To better understand the semiconductor characteristics of **1**, density functional theory (DFT) was utilized to calculate the electronic band structure and partial density of states (PDOS). Fig. 5b illustrates that the maximum valence band value and the bottom of the conduction band value are coercively positioned at the G-spot, proving that **1** is a direct band-gap material. As well, the calculated band gap of **1** according to the DFT is about 2.54 eV [45], which is in good agreement with the experimental result. This value is significantly less than that of other inorganic semiconductors, such as Cr_2O_3 (3.5 eV), ZnO (3.2 eV), and GaN (3.39 eV), comparable to other 2D organic-inorganic hybrid perovskites [46]. Additionally, the PDOS suggest that Bi 6p orbitals dominate the conduction band minimum, and both Cu 4s and Br 4p states account for the valence band maximum (Fig. 5c). It is clear that the inorganic framework primarily controls the optical bandgap and electronic structure of **1**, which is additionally confirmed by its highest occupied molecular orbitals (HOMO) and lowest unoccupied molecular orbitals (LUMO) (Fig. 5d). Further, we also measured the photoelectric response of compound **1**. As shown in Fig. S7 (Supporting information), **1** shows weak photo-

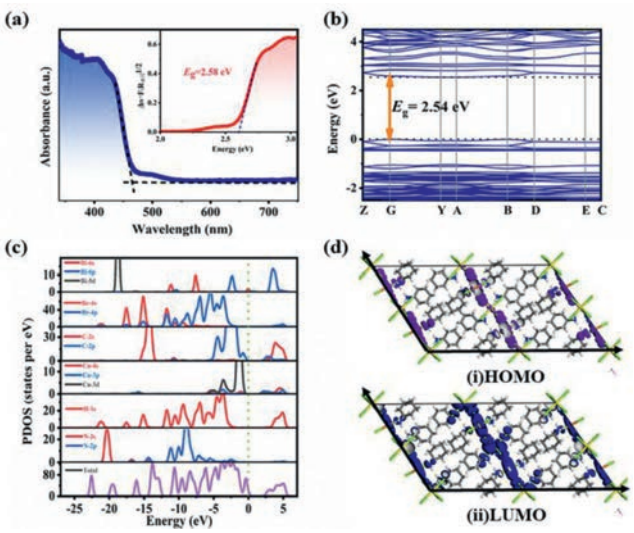

Fig. 5. (a) The UV–vis absorption spectra of **1**, with the band gap deduced from the *Tauc* plot indicated in the inset. (b) Calculated band structure and (c) partial density of states (PDOS) of **1**. (d) Charge-density isosurfaces calculated for HOMO and LUMO orbitals of **1**.

electric response to light illumination, which are similar to other reported 2D double perovskites, such as $(C_3H_9NI)_4AgBiI_8$ [47] and $(C_6H_{16}N_2)_2CuBiI_8$ [48].

In summary, we have successfully designed a lead-free hybrid double perovskite of $(CHA)_4CuBiBr_8$ that serves as the molecular dielectric switch material. It undergoes an invertible phase transition at 378 K induced by ordered-disordered transformation of the organic CHA^+ moiety and distortion of inorganic framework, which gives rise to excellent dielectric switchable performance. That is, its dielectric constants could be switched and tuned between high-dielectric and low-dielectric states. The dielectric signals transitioned between the high and low states without any degradation after multiple cycles indicate its excellent durability. These findings shed light on the further design of molecular dielectric switches in the family of hybrid double perovskites.

Declaration of competing interests

The authors declare that they have no known competing financial interests or personal relationships that could have appeared to influence the work reported in this paper.

Acknowledgments

This work was financially supported by National Natural Science Foundation of China (Nos. 22125110, 22205233, 22193042, 21833010, 21921001, and U21A2069), the Key Research Program of Frontier Sciences of the Chinese Academy of Sciences (No. ZDBS-LY-SLH024), the National Postdoctoral Program for Innovative Talents (No. BX2021315), the National Key Research and Development Program of China (No. 2019YFA0210402), the China Postdoctoral Science Fund (No. 2022TQ0337). Fujian Science & Technology Innovation Laboratory for Optoelectronic Information of China (No. 2021ZR126).

Supplementary materials

Supplementary material associated with this article can be found, in the online version, at doi:10.1016/j.cclet.2023.108707.

References

[1] M. Mączka, A. Gagor, J.K. Zaręba, et al., Chem. Mater. 32 (2020) 4072–4082.
[2] O. Sato, Nat. Chem. 8 (2016) 644–656.
[3] W. Fujita, K. Awaga, J. Solid State Chem. 159 (2001) 451–454.
[4] D.W. Fu, H.L. Cai, Y.M. Liu, et al., Science 339 (2013) 425–428.
[5] C. Shi, X. Zhang, Y. Cai, Y.F. Yao, W. Zhang, Angew. Chem. Int. Ed. 54 (2015) 6206–6210.
[6] Z.X. Zhang, C.Y. Su, J. Li, et al., Chem. Mater. 33 (2021) 5790–5799.
[7] Z.H. Sun, S.Q. Zhang, C.M. Ji, et al., J. Mater. Chem. C 2 (2014) 10337–10342.
[8] D.W. Fu, J.X. Gao, W.H. He, et al., Angew. Chem. Int. Ed. 59 (2020) 17477–17481.
[9] W. Li, C.T. He, Y. Zeng, et al., J. Am. Chem. Soc. 139 (2017) 8086–8089.
[10] S.G. Han, J. Zhang, B. Teng, et al., J. Mater. Chem. C 5 (2017) 8509–8515.
[11] K.W. Tao, S.G. Han, C.M. Ji, et al., Cryst. Growth Des. 18 (2018) 7316–7322.
[12] T. Yang, B. Teng, S.G. Han, et al., Inorg. Chem. Front. 6 (2019) 1761–1766.
[13] Y.Z. Wang, Z.X. Zhang, C.Y. Su, et al., Dalton Trans. 50 (2021) 3841–3847.
[14] B. Bednarska-Bolek, J. Zaleski, G. Bator, R. Jakubas, J. Phys. Chem. Solids. 61 (2000) 1249–1261.
[15] T. Hang, W. Zhang, H.Y. Ye, R.G. Xiong, Chem. Soc. Rev. 40 (2011) 3577–3598.
[16] A. Pietraszko, B. Bednarska-Bolek, R. Jakubas, P. Zielinski, J. Phys. Condens. Mat. 13 (2001) 6471–6488.
[17] Y. Liu, H.J. Xu, X.T. Liu, et al., Chem. Sci. 13 (2022) 13499–13506.
[18] L.N. Hua, L.W. Tang, Y. Liu, et al., Small (2023) e2207393.
[19] L.W. Tang, H.X. Chen, Y. Ma, et al., Inorg. Chem. Front. 9 (2022) 637–644.
[20] S.M. Liu, L. He, Y.Z. Wang, P.P. Shi, Q. Ye, Chin. Chem. Lett. 33 (2022) 1032–1036.
[21] Y.Y. Yu, P.Z. Huang, Y.Z. Wang, et al., Chin. Chem. Lett. 33 (2022) 2143–2146.
[22] M.J. Yang, H. Cheng, Y.Q. Xu, M.Z. Li, Y. Ai, Chin. Chem. Lett. 32 (2021) 3558–3561.
[23] S.G. Han, Y. Ma, L.N. Hua, et al., J. Am. Chem. Soc. 144 (2022) 20315–20322.
[24] S.M. Liu, Y.J. Cao, L. He, P.P. Shi, Q. Ye, Inorg. Chem. 59 (2020) 18396–18401.
[25] A. Zeb, Z.H. Sun, A. Khan, et al., Inorg. Chem. Front. 5 (2018) 897–902.
[26] T. Khan, M.A. Asghar, Z.H. Sun, et al., J. Mater. Chem. C 5 (2017) 2865–2870.
[27] C.M. Ji, Z.H. Sun, S.Q. Zhang, et al., J. Mater. Chem. C 2 (2014) 567–572.
[28] W.C. Zhang, Z.H. Sun, J. Zhang, et al., J. Mater. Chem. C 5 (2017) 9967–9971.
[29] M.M. Lun, F.L. Zhou, D.W. Fu, Q. Ye, J. Mater. Chem. C 10 (2022) 11371–11378.
[30] X. Zheng, L. Zhou, P.P. Shi, et al., Chem. Commun. 53 (2017) 7756–7759.
[31] Y. Zhang, H.Y. Ye, W. Zhang, R.G. Xiong, Inorg. Chem. Front. 1 (2014) 118–123.
[32] A.H. Slavney, T. Hu, A.M. Lindenberg, H.I. Karunadasa, J. Am. Chem. Soc. 138 (2016) 2138–2141.
[33] E.T. McClure, M.R. Ball, W. Windl, P.M. Woodward, Chem. Mate. 28 (2016) 1348–1354.
[34] Y. Bekenstein, J.C. Dahl, J. Huang, et al., Nano. Lett. 18 (2018) 3502–3508.
[35] F.X. Wei, Z.Y. Deng, S.J. Sun, et al., Chem. Commun. 55 (2019) 3721–3724.
[36] F.X. Wei, Z.Y. Deng, S.J. Sun, et al., Chem. Mater. 29 (2017) 1089–1094.
[37] X.T. Liu, Z.Y. Xu, P.Q. Long, et al., Chem. Mater. 32 (2020) 8965–8970.
[38] Y. Liu, Y. Ma, X. Zeng, et al., Nat. Commun. 14 (2023) 2420.
[39] W.Q. Guo, X.T. Liu, S.G. Han, et al., Angew. Chem. Int. Ed. 59 (2020) 13879–13884.
[40] Y. Liu, Z.Y. Wu, X.T. Liu, et al., Adv. Optical. Mater. 7 (2019) 1901049.
[41] Y. Liu, S.G. Han, J.Q. Wang, et al., J. Am. Chem. Soc. 143 (2021) 2130–2137.
[42] K. Aizu, J. Phys. Soc. Jpn. 27 (1969) 387–396.
[43] P.P. Shi, Y.Y. Tang, P.F. Li, et al., Chem. Soc. Rev. 45 (2016) 3811–3827.
[44] D.B. Litvin, Acta Crystallogr. A 64 (2008) 316–320.
[45] G. Kortüm, W. Braun, G. Herzog, Angew. Chem. Int. Ed. 75 (1963) 653–661.
[46] J. Simon, Z. Zhang, K. Goodman, et al., Phys. Rev. Lett. 103 (2009) 26801–26806.
[47] Y.P. Yao, B. Kou, Y. Peng, et al., Chem. Commun. 56 (2020) 3206–3209.
[48] Y.Y. Wang, G.M. Lin, B. Su, et al., Dalton Trans. 51 (2022) 10234–10239.